THE JOURNAL OF PHYSICAL CHEMISTRY C

Article

Cite This: J. Phys. Chem. C 2020, 124, 17−24

pubs.acs.org/JPCC

Molecular Control of Charge Carrier and Seebeck Coefficient in Hybrid Two-Dimensional Nanoparticle Superlattices

Cliff E. McCold,[†] Lucas Domulevicz,[‡] Zhengxu Cai,[§] Wai-Yip Lo,[§] Sahar Hihath,[‡] Katia March,[∥] Hashem M. Mohammad,[⊥] M. P. Anantram,[⊥] Luping Yu,[§] and Joshua Hihath*[,‡]

[†]Materials Science and Engineering, University of California, Davis, Davis, California 95616, United States

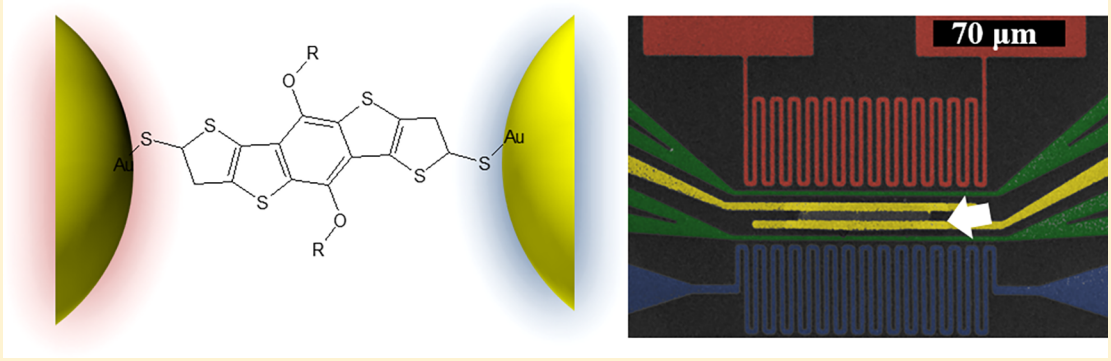
[‡]Electrical and Computer Engineering, University of California, Davis, Davis, California 95616, United States

[§]Department of Chemistry and the James Franck Institute, The University of Chicago, Chicago, Illinois 60637, United States

[∥]Eyring Materials Center, Arizona State University, Tempe, Arizona 85280, United States

[⊥]Electrical and Computer Engineering, University of Washington, Seattle, Washington 98195, United States

Supporting Information



ABSTRACT: The development of high efficiency thermoelectric materials would revolutionize energy harvesting capabilities and be useful for a large number of applications. Hybrid organic−inorganic nanostructured materials are an intriguing platform for developing efficient thermoelectric systems due to the possibility of independently controlling the thermal and electrical conductivity of the material with intelligent choices for material components. In this study we control the thermopower of hybrid 2-dimensional (2D) nanoparticle−molecule superlattices by systematically modifying molecular properties. Five conjugated, ladder-type, heteroacene molecules are used to interlink gold nanoparticles and control the thin films' properties. Interestingly, we measure a change in the sign of the Seebeck coefficient, corresponding to a crossover of the majority charge carrier (from hole to electron). Hall-effect measurements are used to confirm the change in dominant carrier for these systems. And density functional theory (DFT) is used in combination with Green's function-based transport calculations to examine the energy level-alignments in the system. The single−molecule Seebeck coefficient predictions from these results compare favorably with the experimental results of the molecular arrays and provide potential insights into the origins of the sign-change of the carriers in the system. In addition, the thermoelectric power factor σS^2 is found to range above predicted values for hybrid systems and to deviate from optimization strategies for conventional materials. A simple strategy to further increase σS^2 is highlighted. Limitations of the model and sources of variability in the experimental results are discussed. Our findings develop a stronger understanding of charge transport in molecule−nanoparticle hybrid films; demonstrate that these hybrid materials allow facile control over both the carrier type and the power factor of the material, both of which are important for maximizing the efficiency of functional thermoelectric devices; and establish a framework for continuing to maximize the thermoelectric efficiency of these materials.

INTRODUCTION

Nanoparticle−molecule arrays are promising materials for a variety of applications due to their highly tunable structure and unique electronic transport properties.[1] In particular, astute selection of interparticle molecular linkers can create arrays with high electrical and low thermal conductivity.[2] The ability to decouple charge and phonon transport originates from the tunneling nature of charge transport from particle to particle, the relatively low thermal conductivity of organic molecules, and the significant mismatch in vibrational mode energies between the nanoparticles (NP) and the molecules. This set of properties is exactly what is desired in thermoelectric materials,

Received: August 27, 2019
Revised: November 21, 2019
Published: December 9, 2019

Downloaded via UNIV OF WASHINGTON on September 13, 2024 at 21:56:24 (UTC).
See https://pubs.acs.org/sharingguidelines for options on how to legitimately share published articles.

© 2019 American Chemical Society

DOI: 10.1021/acs.jpcc.9b08185
J. Phys. Chem. C 2020, 124, 17−24

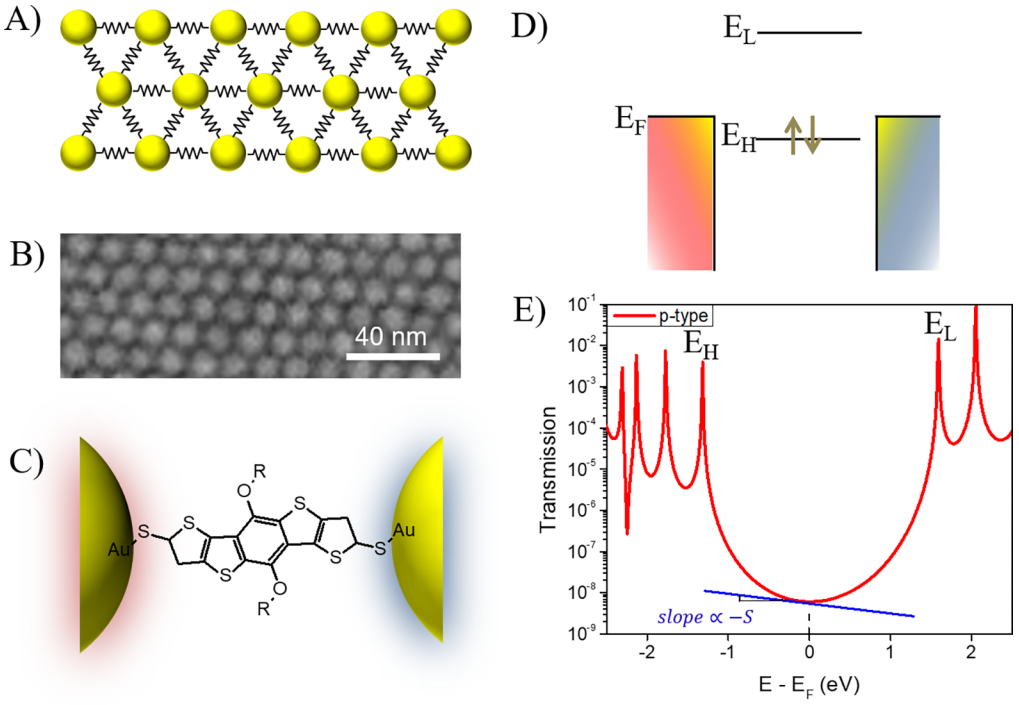


Figure 1. Schematic of NP array, molecular junction, energy band diagram, and transmission probability. (A) Schematic of a two-dimensional nanoparticle−molecule array, with molecules acting as resistors connecting each node (nanoparticle) in the resistive network. (B) Scanning electron microscope (SEM) image of the NP−molecule array in Oleylamine-capped state. (C) Heteroacene 5 (HA5) molecule bridging between hot (red) and cold (blue) nanoparticles. (D) Energy-level diagram for a molecule−nanoparticle junction with the HOMO level (E_H) in close proximity to the Fermi level (E_F). (E) Transmission function versus $E - E_F$ for a molecular junction (HA11), where a negative slope of $d\mathcal{T}/dE$ at $E = E_F$ imparts a positive value to the Seebeck coefficient, indicating hole transport through the more proximal HOMO.

as can be seen in the thermoelectric figure of merit, $ZT = \frac{S^2\sigma T}{\kappa}$.[3] In this expression, S is the Seebeck coefficient, σ is the electrical conductivity, T is the temperature, and κ is the thermal conductivity. A high electrical conductivity and a low thermal conductivity can give a high ZT if the Seebeck coefficient can also be optimized. It is generally recognized that a ZT over 4 would mark a significant breakthrough,[3,4] and ZT's over 10 have been predicted for nanoparticle−molecule arrays.[2] Historically, measuring the thermal conductivity of individual molecules has been very difficult, but recent advances[5] would allow experimental determination of κ and make empirical determination of ZT even more promising for future work on thermoelectric hybrid molecular materials.

A nanoparticle−molecule superlattice acts like a network of resistors (Figure 1A), where nanoparticles are the network nodes and molecular linkers determine the interparticle resistances.[6] Because of this, the molecules play a dominant role in the transport properties of the system.[6,7] Self-assembly of monolayers of these nanoparticle−molecule arrays enables facile transfer of these structures to surfaces for thermal and electrical characterization (Figure 1B).[8−10] The role of the molecule is 3-fold: (i) the nanoparticle surfaces are stabilized by the molecules that prohibit aggregation and determine particle separation (Figure 1C); (ii) molecular energy levels determine the tunneling barrier between adjacent particles (Figure 1D) and thus determine the electrical conductivity of the film; and (iii) the alignment between the molecular and nanoparticle energy levels determines the thermovoltage obtained in the films. The transmission function characterizes the probability of successful transfer of a charge carrier from one side of a molecular junction to the other (Figure 1E) and indicates the influence of the position of the molecular energy levels on charge transport. The highest occupied molecular orbital (HOMO) and lowest unoccupied molecular orbital (LUMO) have energies of E_H and E_L, respectively. The orbital with the energy closest to the Fermi energy of the nanoparticle will determine the majority charge carrier of the junction, with the HOMO supporting hole transport and the LUMO supporting electron transport. And, the closer either of these orbitals are to the chemical potential (Fermi Energy) of the nanoparticles, the higher the conductance will be.

In addition to dictating the electrical conductivity of the film, the alignment between the dominant molecular energy level and the nanoparticle chemical potential also influences the thermoelectric properties. The Seebeck coefficient quantifies a material's thermoelectric potential and is defined as $S = -\frac{V_{hot} - V_{cold}}{T_{hot} - T_{cold}}$, where V_{hot} and T_{hot} are the voltage and temperature of the hot side of a thermoelectric material, respectively. In a bulk n-type material the Fermi distribution will be broader on the hot side, yielding more electrons at higher energies, which will diffuse away faster than less energetic cold electrons can replace them.[11] This creates a positive potential at the hot side, leading to a positive value for ΔV and a negative Seebeck coefficient, and indicates majority electron transport. Because this property of the Seebeck coefficient is preserved in nanostructured materials and molecular junctions,[12] the Seebeck coefficient provides insight into the majority charge carrier in NP−molecule arrays. For molecular tunnel junctions, the Seebeck coefficient captures the sign of the majority charge carrier through the slope of the transmission function,[13,14]

DOI: 10.1021/acs.jpcc.9b08185
J. Phys. Chem. C 2020, 124, 17−24

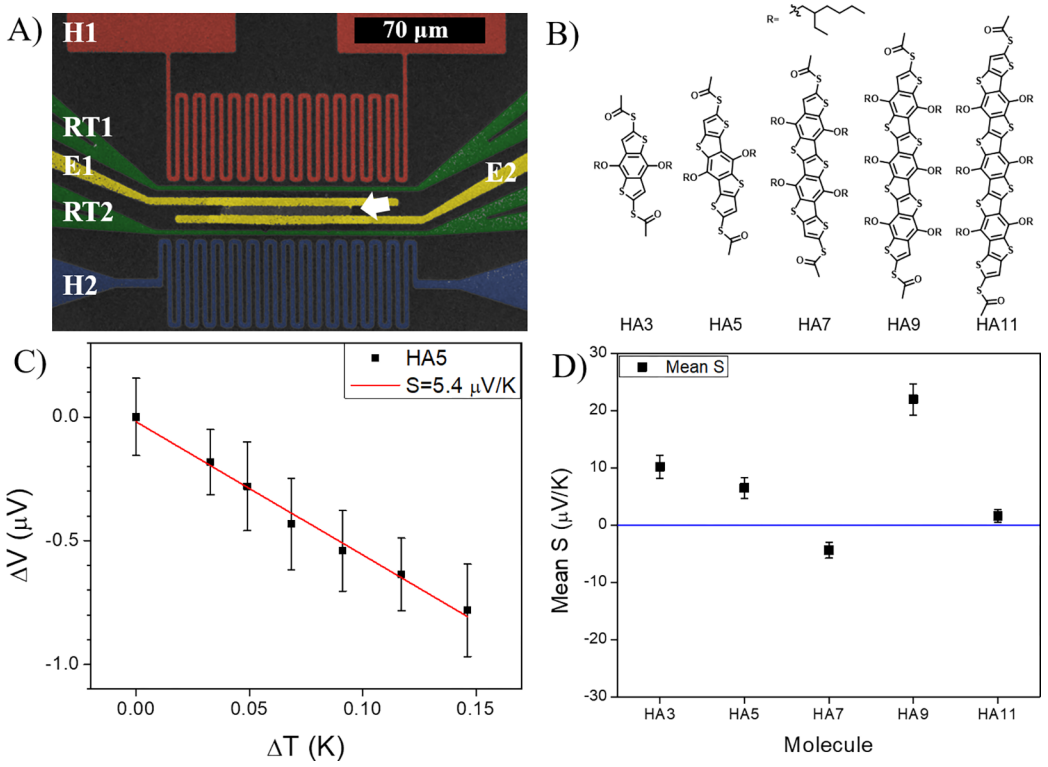


Figure 2. Device platform, molecular series, and thermoelectric results. (A) Thermoelectric chip platform with the heated on-chip heater (red, H1), two resistive thermometers (green, RT1,2), the hot electrode 1 (yellow, E1), the cold electrode 2 (yellow,E2), and a second unheated on-chip heater (blue, H2). An arrow points to the NP−molecule superlattice. (B) The five ladder-type heteroacene molecules used in this study, from left to right, HA3, HA5, HA7, HA9, HA11. (C) Representative $\Delta V-\Delta T$ plot for HA5 taken from measurements on the thermoelectric chip platform. The slope of the line indicates a Seebeck coefficient of 5.4 μV/K. (D) Measured Seebeck coefficients for nanoparticle−molecule arrays for each of the five heteroacene molecules. Each data point represents the mean from 18 separate devices. Error bars are standard error of the mean.

$$S_{\text{junction}} = -\frac{\pi^2 k_B^2 T}{3e}\frac{\partial \ln \mathcal{T}(E)}{\partial E}\Big|_{E=E_F} \quad (1)$$

where k_B is Boltzmann's constant, e is the elementary charge, E is the energy of the charge carrier, E_F is the Fermi level, and $\mathcal{T}(E)$ is the transmission function. For a molecular junction, a HOMO level that is closer to the Fermi energy imparts a negative value to $\delta \ln \mathcal{T}(E)/\delta E$ and a positive value to S_{junction}, corresponding to hole-type transport (Figure 1E). Importantly, as either of the energy levels moves closer to E_F, not only does the conductance increase but so does the magnitude of the Seebeck coefficient, thus simultaneously increasing both factors.[15] In the case of a nanoparticle array, because of the resistive network nature of the system, it is expected that[2,16]

$$S_{\text{NPA}} \approx S_{\text{junction}} \quad (2)$$

where S_{NPA} is the Seebeck coefficient for the nanoparticle−molecule array. Thus, by measuring the Seebeck coefficient of self-assembled nanoparticle arrays, we gain insight into the average thermoelectric properties of the nanoparticle−molecule−nanoparticle junctions, including the majority charge carrier, and the relative position of the molecular frontier orbitals to the chemical potential of the nanoparticles.

In the following we examine the electrical conductivity, Seebeck coefficient, and power factor for a series of hybrid, 2D, molecule−nanoparticle superlattices. In these monolayer films, we demonstrate that it is possible to change the type of charge carrier to obtain either electron or hole dominated transport. This places these systems in stark contrast with traditional organic thermoelectrics where n-type conduction has been difficult to obtain.[17−20] The development of high-quality, n-type thermoelectric materials is key for developing real-world devices where n-type and p-type materials must be combined to maximize efficiency.[19,21] Finally, we demonstrate that the power factor increases with conductivity, suggesting even higher power factors are obtainable. The combination of these feature makes these hybrid, nanostructured materials intriguing systems for the continued development of thermoelectrics.

RESULTS AND DISCUSSION

In order to understand the effects of molecular properties on the thermoelectric performance of hybrid superlattices, we created monolayer arrays of nanoparticles that were interlinked with each of the five ladder-type heteroacene molecules shown in Figure 2B (HA3 through HA11). The heteroacene molecules were introduced to the arrays via solution phase ligand exchange. Seebeck coefficients were measured for 18 NP−molecule array thermoelectric devices for each of the heteroacene molecules (90 devices in total). A false-color SEM micrograph of the thermoelectric measurement platform is shown in Figure 2A. An on-chip heater (H1) creates a local temperature gradient when subjected to an applied current. Two on-chip resistive thermometers (RT1, RT2) are used to calibrate the temperature gradient at each of the applied heater currents. Two electrodes (E1, E2) contact opposite sides of a 70 μm × 4 μm NP−molecule monolayer array, and a lab-constructed instrumentation amplifier measures the thermovoltage between these two electrodes. The cold heater (H2) is unused during all measurements but enables checks for

DOI: 10.1021/acs.jpcc.9b08185
J. Phys. Chem. C 2020, 124, 17−24

symmetric behavior. Similar techniques have been used before to measure nanowires[22,23] and bulk nanocrystal solids.[24] Further details on methods are available in the Supporting Information.

A typical measurement of the Seebeck coefficient of one device is shown in Figure 2C. Applied heater currents create temperature gradients from 0 to 0.15 K across the 4 μm NP−molecule array, and thermovoltages up to 1 μV are recorded. The five heteroacene molecules are planar, highly conjugated, and composed of fused thiophenes and benzothiophenes (Figure 2B). The mean Seebeck coefficients from 18 measurements are presented for superlattices in each of the molecular states (Figure 2D). Interestingly, the change in the Seebeck is not monotonic. Positive Seebeck coefficients, and thus p-type transport, are observed for heteroacenes with 3, 5, 9, and 11 rings (HA3, HA5, HA9, HA11), while a large negative Seebeck coefficient is observed for the HA7 superlattice. Holes are expected to be the dominant carrier for the entire molecular series, with HOMOs expected to be much closer to E_F than LUMO;[25] thus this change in charge carrier across the molecular series indicates significant differences in the alignment of the frontier orbitals with the chemical potential of the nanoparticles compared to that of bulk electrodes.

To verify the sign of the charge carrier in these devices, we turned to Hall-effect measurements. Briefly, Hall-effect measurements work by applying a magnetic field, **B**, normal to the device plane while applying a current I through the device. The deflection of charge carriers in the magnetic field creates a voltage perpendicular to the direction of current, and this is the Hall voltage. The sign of the Hall coefficient corresponds to the sign of the Hall voltage and thus the sign of the charge carrier. To measure this effect, custom devices were fabricated with a cloverleaf-style Van der Pauw geometry.[26] Due to the ∼1 mm separation of Hall device electrodes and the difficulty in forming macrostructurally connected monolayers of this size, trilayer superlattices were used instead of monolayer arrays for the Hall-effect measurements. Superlattices were stamped on the custom substrates and exchanged to each of the five heteroacene molecular states (Figure 3B). The Hall-effect measurements were performed on a LakeShore Cryotronics 8400 HMS with a DC magnetic field of 1.7 T. For devices in each molecular sate, Hall voltages, V_H, were measured at three applied currents, and the Hall coefficients were then calculated using $R_H = V_H t/I\mathbf{B}$, where t is film thickness, I is applied current, and **B** is the magnetic field. The Hall-effect measurements on the heteroacene superlattices (Figure 3A) generally agree with the sign of the charge carrier observed in the Seebeeck coefficients and confirm that the HA7 case is dominated by electron transport while most of the other films are dominated by holes. The exception is the HA9 case, where the Seebeck coefficient suggests hole transport, and the Hall measurements suggest electron transport. This discrepancy may be due to macrostructural effects in the films, such as the difference between the monolayer thermoelectric samples and trilayer Hall-effect samples, or the fact that the chemical potential is near the midgap between the HOMO−LUMO levels as is discussed below.[27−30] Hall-effect measurements on nanoparticle superlattices are not without difficulties, and further information about the measurement approach, including Hall carrier mobility and sheet carrier concentration, are available in the Supporting Information in section 4.

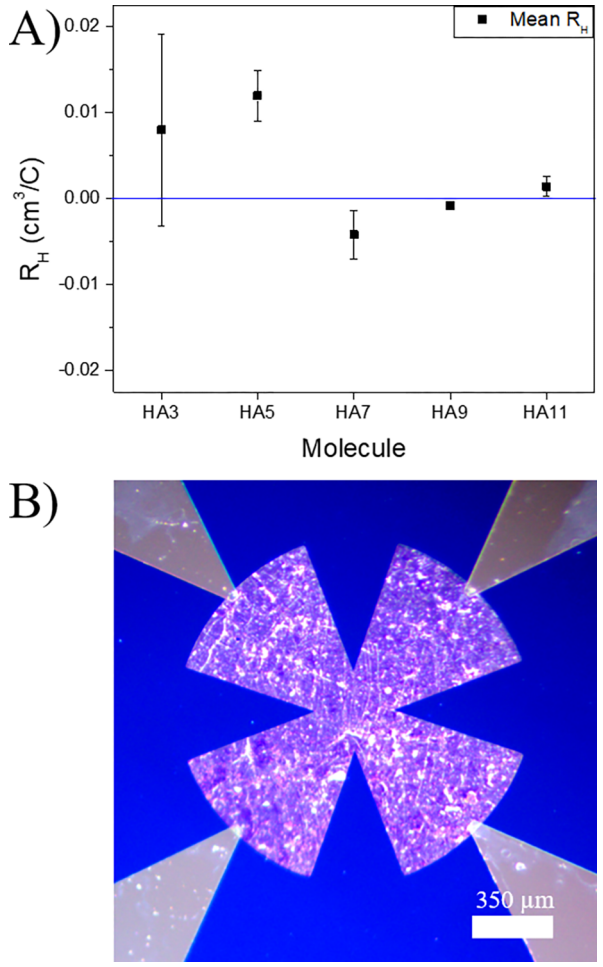


Figure 3. Hall-effect characterizations. (A) Measured Hall coefficients, R_H, for nanoparticle arrays in the five molecular states. Each data point represents the mean of at least 12 DC Hall measurements, four at three different applied currents. Error bars are standard deviation of the mean. (B) Optical microscope image of a typical Hall-effect device with 4 Au electrodes contacting the NP−molecule array in a Van der Pauw cloverleaf geometry. The blue substrate is silicon nitride. The array minimum width and scale bar are 350 μm. Variations in the brightness of the NP−molecule array indicate inhomogeneities in the NP film that are unavoidable with millimeter size arrays.

To understand why there is a change in the charge carrier in these films, we next examine the electronic properties of the systems using a combination of optical absorbance and density functional theory (DFT). The optical absorbance onset peak in these molecules exhibit a significant red shift as the molecular length increases from HA3 to HA11 (Figure 4A). This shift corresponds to a decrease in the energy gap between the HOMO−LUMO levels as the molecular length increases, as expected for extended conjugated systems like the heteroacenes. Interestingly, there is a significant change in the absorption energy between the HA5 and HA7 cases.

The trend indicated by these experimental absorption onset peaks matches the change in the energy levels calculated using DFT. The electronic structure of each of the molecules was calculated using the B3LYP functional and the 6-31G(d,p) basis set in Gaussian 09W.[31] Figure 4B shows the HOMO and LUMO levels calculated using DFT for each of the five HA molecules. To obtain the results discussed above with the

DOI: 10.1021/acs.jpcc.9b08185
J. Phys. Chem. C 2020, 124, 17−24

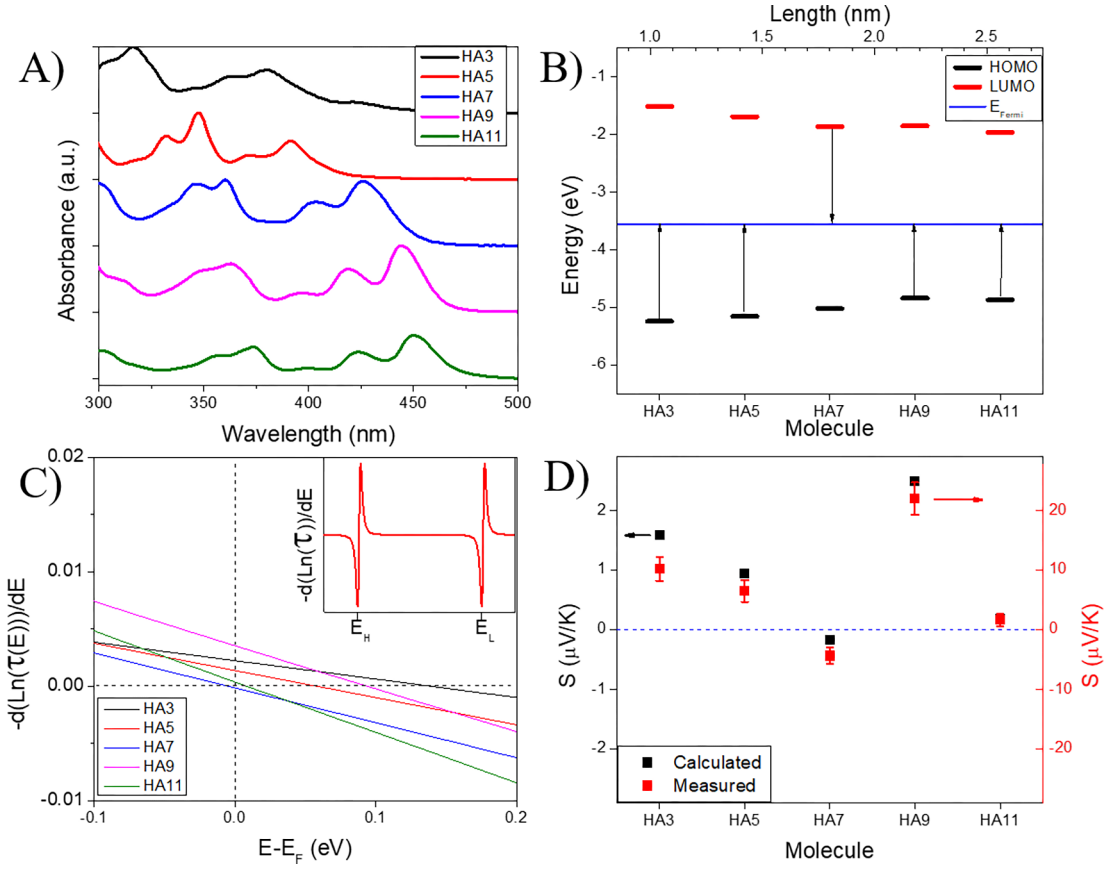


Figure 4. Molecular energy levels and calculated Seebeck coefficients. (A) Absorbance spectra for the five heteroacene molecules, with increasing wavelength of absorption onset indicating decreasing HOMO−LUMO gap as molecular length increases. (B) $E - E_F$ for HOMO and LUMO energy levels for the five molecules, with arrows indicating the energy levels closest to E_F. (C) Negative derivatives ($-\mathrm{d}\ln \mathcal{T}/\mathrm{d}E$) of the transmission functions for each molecule calculated using eq 1. The sign of $-\mathrm{d}\ln \mathcal{T}/\mathrm{d}E$ at $E - E_F$ to the Seebeck coefficient sign. The inset is an idealized plot of $-\mathrm{d}\ln \mathcal{T}/\mathrm{d}E$ for a representative molecule over a wider range of energies showing the shape of the derivative. (D) Calculated Seebeck coefficients (black) for single molecule junctions from eq 1 and measured Seebeck coefficients (red). Error bars on measured Seebeck coefficient are standard error of the mean from 18 samples.

negative Seebeck coefficient and charge carrier in the HA7 case, the chemical potential of the nanoparticles must be closer to the LUMO level in the HA7 case and closer to the HOMO level in the other cases. To examine this possibility, we have calculated the transmission functions for the molecular junctions using Green's function-based transport calculations (see Figure S2 and section 2 of the Supporting Information for details).[32] From these transmission functions, we obtain the Seebeck coefficients using eqs 1 and 2 above (Figure 4C,D). Because the alignment between the molecular energy levels and nanoparticle chemical potential is generally unknown, we then use the Fermi energy as a fitting parameter, to determine if there is a range where a negative Seebeck coefficient is observed for HA7 and positive values for the other molecules. We find that in the range of $-3.572 < E_F < -3.558$ eV, this condition can be obtained (Figure 4B). Importantly, this indicates that in all cases the chemical potential of the nanoparticles is pinned near the midgap between the HOMO and LUMO levels. This is significantly different from what is generally obtained when a molecule is bound between bulk Au electrodes, where with thiolated molecules the HOMO level tends to be closer to the Fermi energy.[25] This difference in the Fermi energy is likely due to a combination of the difference in size between the nanoparticles and bulk systems, the effect of surface interactions between the Au and the amines and thiols, and the surface structure of the nanoparticles.[33,34] This result suggests that the most important factor for improving the thermoelectric properties of 2D nanoparticle films will be designing molecules and linkers that will allow one energy level to be significantly closer to the nanoparticle chemical potential after interlinking the molecules.

We also note that within the range of chemical potentials above, the overall trend of the calculated Seebeck coefficients match well with the experimental results (Figure 4D, black and red, respectively), as both the sign of the carriers and the relative changes of the Seebeck coefficients can be reproduced. While analysis with this simple model is not quantitative, it clearly indicates that the complex behavior of the Seebeck coefficient in this series of NP superlattices is due to changes in the molecular properties. In addition, it confirms that the type of charge carriers can be easily modified in these arrays, pointing to the possibility of developing combined n- and p-type thermoelectric devices as is necessary for practical applications.

Having understood the origin of the behavior of the Seebeck coefficient from a molecular perspective, we next turn to the influence of the Seebeck coefficient on the total thermoelectric performance of the material by examining the thermoelectric power factor σS^2. The thermoelectric power factor σS^2 defines the numerator of the figure of merit (ZT) and thus offers

DOI: 10.1021/acs.jpcc.9b08185
J. Phys. Chem. C 2020, 124, 17−24

significant insight into the expected behavior of a material's thermoelectric performance, while capturing the important influence of electrical conductivity on these properties. Figure 5A indicates the typical behavior of σ, S, and σS^2 in bulk materials as a function of an idealized physical coordinate such as charge carrier concentration.[3] For most bulk or nanostructured materials increasing the carrier concentration not only increases σ but also causes a decrease in S, which implies there will be a maximum value for the power factor.[3,18,35] The conductivity σ is an important part of the power factor and understanding the thermoelectric performance of the hybrid films. Because the conductivity of the NP−molecule film depends on the particle separation, any polydispersity in particle size leads invariably to disruptions in the long-range crystalline packing of the particles. Particle polydispersity thus leads to a distribution of interparticle separations. The effect of particle separation distributions on electrical conductivity is compounded by sample-specific macrostructural effects (aggregations and voids) and ligand exchange variables.[36,37] Because of these factors, a broad distribution of conductance values in NP−molecule arrays is almost unavoidable in macroscopic films. Further information about the conductivity and structural properties of the films, including particle separation distributions and ligand exchange efficiencies, is available in Supporting Information sections 3, 5, and 6. Having measured both σ and S for 90 distinct thermoelectric nanoparticle−molecule array devices, we examine the measured thermoelectric power factor σS^2.

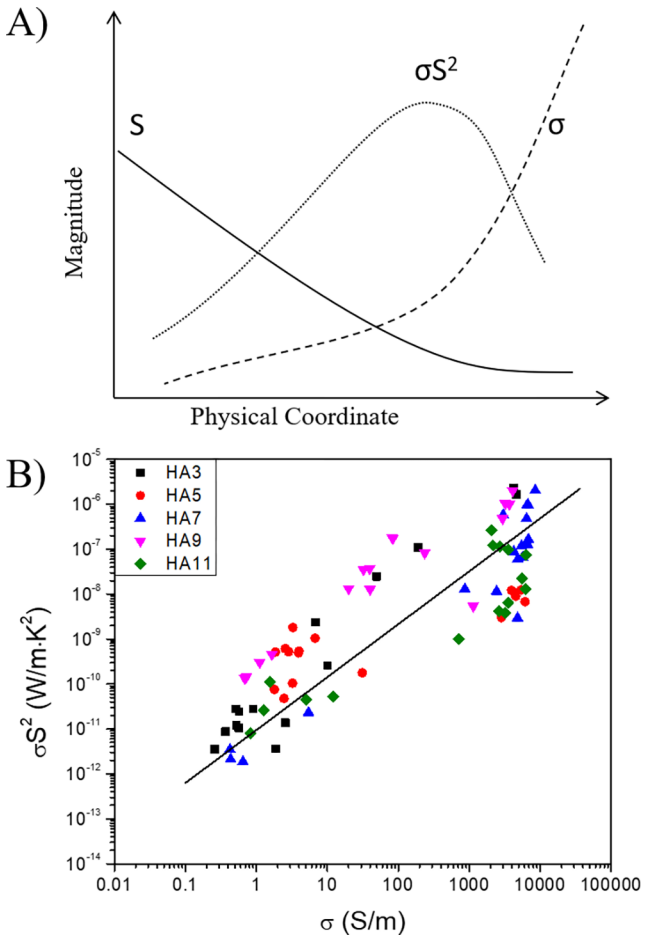


Figure 5. Thermoelectric power factor of NP molecule arrays. (A) Illustrative schematic indicating typical behavior of S, σ, and the power factor σS^2 in bulk materials as a function of an idealized physical coordinate such as charge carrier concentration. (B) Experimentally obtained thermoelectric power factor σS^2 vs σ indicating a broad distribution but increasing trend, suggesting the maximum value of σS^2 has not been reached for this system. The solid line is a guide to the eye.

The broad range of Seebeck and conductivity values observed in our data set can been seen in Figure 5B in power factors ranging from 10^{-12} to 10^{-6} W/(m·K^2). In the literature, experimental power factors of nanoparticle arrays ranging from 10^{-16} to 10^{-8} have been reported,[16] and theoretical predictions of the normalized power factor have been around 10^{-4} W/(m·K^2).[2] Interestingly, we observe no decrease in the power factor as conductivity increases over a range of 4 orders of magnitude. This promising result suggests that these NP−molecule arrays have yet to reach the maximum possible power factor. In fact, contrary to conventional systems, the Seebeck coefficient is expected to increase in concert with the molecular conductance, pointing to a clear strategy to maximize the thermopower of these NP molecule arrays.

The intriguing advantage of hybrid nanoparticle−molecule array systems over conventional materials is the determination of both conductivity and Seebeck coefficient by the molecular linkers. In fact, shifting the Fermi level closer to a frontier orbital should dramatically increase S, by increasing the slope of the transmission function at E_F, and simultaneously, significantly increase σ, by reducing the height of the tunneling barrier. This synergistic effect implies that simply controlling the position of the molecular frontier orbitals relative to E_F via either gating or chemical methods will allow dramatic increases in thermopower. This ability to improve both S and σ should in principle allow high ZT values even if the heat transport is dictated by the Weidemann−Franz law.[38,39]

CONCLUSION

Control of the Seebeck coefficient and the sign of the majority charge carrier is demonstrated using five heteroacene molecular linkers in nanoparticle−molecule monolayer arrays. The charge carrier sign is confirmed using Hall-effect measurements and a single molecule transmission formalism supports the change in sign of the majority charge carrier in this system. The thermoelectric power factor σS^2 increases with σ, suggesting that the maximum thermopower of these materials has yet to be achieved. In total, these results suggest a clear strategy to further increase thermoelectric power of these materials by closely aligning E_F with frontier orbital energies using gating. This strategy maximizes the Seebeck coefficient by increasing the slope of the transmission function and increases σ by reducing the height of the interparticle tunneling barrier.

High power factors, combined with expected low thermal conductivity suggest that high ZT values should be possible in this system. Moreover, the observation of both p-type and n-type behavior in heteroacene nanoparticle superlattices suggest that building functional thermoelectric devices that require both p-type and n-type materials will be a more tractable problem in hybrid superlattices than it has been for conducting polymer systems. Future work on maximizing the thermoelectric potential of nanoparticle−molecule arrays appears quite promising in light of these results.

DOI: 10.1021/acs.jpcc.9b08185
J. Phys. Chem. C 2020, 124, 17−24

METHODS

Briefly, monolayer nanoparticle arrays (Figure 1B) are self-assembled on a water surface and transferred to photolithographically patterned thermoelectric chips (Figure 2A) using polydimethylsiloxane (PDMS) microcontact printing. Au nanoparticles are synthesized in boiling toluene from tetrachloroauric acid and oleylamine. Further details are in the Supporting Information. As synthesized, these nanoparticles are initially covered with oleylamine ligands. Therefore, to introduce the ladder-type heteroacene molecules (Figure 2C), the nanoparticle−molecule arrays on thermoelectric chips undergo a solution phase ligand exchange at 100 μM heteroacene in tetrahydrofuran.[36] An estimate for the relative exchange efficiency of each heteroacene molecule into the oleylamine arrays is provided in the Supporting Information in section 6. Previously, five heteroacene molecules functionalized with dithiols were synthesized according to published methods.[25,40] These dithiolated molecules link between adjacent nanoparticles and determine the electrical conductivity of the monolayer arrays. An on-chip resistive heater (H1 in Figure 2A) creates a thermal gradient, and two resistive thermometers (RT1, RT2) are used to calibrate the temperature difference (ΔT). A differential instrumentation amplifier measures the thermovoltage (ΔV) between the hot and cold electrodes (E1 and E2). By systematically modifying the applied heater currents, a range of temperature gradients can be measured, allowing the extraction of the Seebeck coefficient from a plot of ΔV vs ΔT (Figure 2B). The differential instrumentation amplifier used for thermoelectric measurements was built using two OPA128 amplifiers and an INA105 differential amplifier with an input impedance of 1E13 Ohms.

Ninety distinct 70 μm × 4 μm nanoparticle monolayer devices were created, and 18 devices underwent ligand exchange into each of the five heteroacene molecules (HA3, HA5, HA7, HA9, and HA11). During a thermoelectric measurement, seven applied heater current settings were used to create seven temperature gradients ranging from 0 to 0.15 K across the 4 μm device. Each device experiences at least five complete thermal gradient cycles (ΔT = 0, 0.04, ..., 0.15 K), and the Seebeck coefficient for each device is calculated from the negative slope of ΔV vs ΔT for those five aggregated measurements. The Seebeck coefficients for the nanoparticle arrays in each molecular state are the mean of 18 such device measurements, which includes the thermovoltage results from at least 90 complete thermal cycles.

Measurements of the Hall coefficient are performed on trilayer nanoparticle arrays on photolithographically patterned chips with a cloverleaf-style Van der Pauw geometry. The device exhibits 90° rotational symmetry and the ratio of the sample−electrode contact length to sample boundary length, λ, is less than 0.086.[26] Further details are in the Supporting Information.

ASSOCIATED CONTENT

Supporting Information

The Supporting Information is available free of charge at https://pubs.acs.org/doi/10.1021/acs.jpcc.9b08185.

Heater calibration, DFT and transport calculations, particle separation statistics, Hall-effect mobility and carrier concentration, conductance of NP arrays, normalized exchange efficiencies, Au nanoparticle and heteroacene syntheses; figures of temperature readings, transmission spectra, distributions of nanoparticle separations, and mean carrier mobility and sheet carrier concentrations (PDF)

AUTHOR INFORMATION

Corresponding Author

*jhihath@ucdavis.edu.

ORCID

Cliff E. McCold: 0000-0002-2463-3828
Zhengxu Cai: 0000-0003-0239-9601
Wai-Yip Lo: 0000-0002-5171-2564
Joshua Hihath: 0000-0002-2949-9293

Notes

The authors declare no competing financial interest.

ACKNOWLEDGMENTS

We acknowledge the U.S. National Science Foundation (CBET-1605338, ECCS-1807391) and Office of Naval Research (N00014-16-1-2658) for financial support. This work was also supported by NSF (Chem-1802274, L.P.Y.) and partially supported by the University of Chicago Materials Research Science and Engineering Center, which is funded by the National Science Foundation under award number DMR-1420709. We acknowledge the Kuwait University Scholarship. We thank Srabanti Chowdhury and Matthew Laurent for their assistance with the Hall-effect measurements.

REFERENCES

(1) Talapin, D. V.; Lee, J.-S.; Kovalenko, M. V.; Shevchenko, E. V. Prospects of Colloidal Nanocrystals for Electronic and Optoelectronic Applications. *Chem. Rev.* **2010**, *110*, 389−458.

(2) Müller, K.-H. Thermoelectrics in an Array of Molecular Junctions. *J. Chem. Phys.* **2008**, *129*, 044708.

(3) Snyder, G. J.; Toberer, E. S. Complex Thermoelectric Materials. *Nat. Mater.* **2008**, *7* (2), 105−114.

(4) Harman, T. C. Quantum Dot Superlattice Thermoelectric Materials and Devices. *Science* **2002**, *297* (5590), 2229−2232.

(5) Cui, L.; Hur, S.; Akbar, Z. A.; Klöckner, J. C.; Jeong, W.; Pauly, F.; Jang, S.; Reddy, P.; Meyhofer, E. Thermal Conductance of Single-Molecule Junctions. *Nature* **2019**, *572*, 628−633.

(6) Zabet-Khosousi, A.; Dhirani, A.-A. Charge Transport in Nanoparticle Assemblies. *Chem. Rev.* **2008**, *108* (10), 4072−4124.

(7) Middleton, A.; Wingreen, N. Collective Transport in Arrays of Small Metallic Dots. *Phys. Rev. Lett.* **1993**, *71* (19), 3198−3201.

(8) Lin, X. M.; Jaeger, H. M.; Sorensen, C. M.; Klabunde, K. J. Formation of Long-Range-Ordered Nanocrystal Superlattices on Silicon Nitride Substrates. *J. Phys. Chem. B* **2001**, *105* (17), 3353−3357.

(9) Liao, J.; Blok, S.; van der Molen, S. J.; Diefenbach, S.; Holleitner, A. W.; Schönenberger, C.; Vladyka, A.; Calame, M. Ordered Nanoparticle Arrays Interconnected by Molecular Linkers: Electronic and Optoelectronic Properties. *Chem. Soc. Rev.* **2015**, *44* (4), 999−1014.

(10) Eah, S.-K. A Very Large Two-Dimensional Superlattice Domain of Monodisperse Gold Nanoparticles by Self-Assembly. *J. Mater. Chem.* **2011**, *21* (42), 16866.

(11) Kasap, S. Thermoelectric Effects in Metals: Thermocouples. In *Principles of Electronic Materials and Devices*; McGraw-Hill Education, 2017.

(12) Cui, L.; Miao, R.; Wang, K.; Thompson, D.; Zotti, L. A.; Cuevas, J. C.; Meyhofer, E.; Reddy, P. Peltier Cooling in Molecular Junctions. *Nat. Nanotechnol.* **2018**, *13*, 122.

DOI: 10.1021/acs.jpcc.9b08185
J. Phys. Chem. C 2020, 124, 17−24

(13) Paulsson, M.; Datta, S. Thermoelectric Effect in Molecular Electronics. *Phys. Rev. B: Condens. Matter Mater. Phys.* **2003**, *67* (24), 241403.
(14) Reddy, P.; Jang, S.-Y.; Segalman, R. a; Majumdar, A. Thermoelectricity in Molecular Junctions. *Science* **2007**, *315* (5818), 1568−1571.
(15) Mahan, G. D.; Sofo, J. O. The Best Thermoelectric. *Proc. Natl. Acad. Sci. U. S. A.* **1996**, *93* (15), 7436−7439.
(16) Chang, W.; Russ, B.; Ho, V.; Urban, J. J.; Segalman, R. a. Gold Nanocrystal Arrays as a Macroscopic Platform for Molecular Junction Thermoelectrics. *Phys. Chem. Chem. Phys.* **2015**, *17*, 6207.
(17) de Leeuw, D. M.; Simenon, M. M. J.; Brown, a. R.; Einerhand, R. E. F. Stability of N-Type Doped Conducting Polymers and Consequences for Polymeric Microelectronic Devices. *Synth. Met.* **1997**, *87*, 53−59.
(18) Russ, B.; Glaudell, A.; Urban, J. J.; Chabinyc, M. L.; Segalman, R. A. Organic Thermoelectric Materials for Energy Harvesting and Temperature Control. *Nat. Rev. Mater.* **2016**, *1* (10), 16050.
(19) Zhang, Q.; Sun, Y.; Xu, W.; Zhu, D. Organic Thermoelectric Materials: Emerging Green Energy Materials Converting Heat to Electricity Directly and Efficiently. *Adv. Mater.* **2014**, *26* (40), 6829−6851.
(20) Yue, R.; Xu, J. Poly(3,4-Ethylenedioxythiophene) as Promising Organic Thermoelectric Materials: A Mini-Review. *Synth. Met.* **2012**, *162* (11−12), 912−917.
(21) Fleurial, J.-P. Thermoelectric Power Generation Materials: Technology and Application Opportunities. *JOM* **2009**, *61* (4), 79−85.
(22) Shi, L.; Li, D.; Yu, C.; Jang, W.; Kim, D.; Yao, Z.; Kim, P.; Majumdar, A. Measuring Thermal and Thermoelectric Properties of One-Dimensional Nanostructures Using a Microfabricated Device. *J. Heat Transfer* **2003**, *125* (5), 881.
(23) Hochbaum, A. I.; Chen, R.; Delgado, R. D.; Liang, W.; Garnett, E. C.; Najarian, M.; Majumdar, A.; Yang, P. Enhanced Thermoelectric Performance of Rough Silicon Nanowires. *Nature* **2008**, *451* (7175), 163−167.
(24) Wang, R. Y.; Feser, J. P.; Lee, J.-S.; Talapin, D. V.; Segalman, R.; Majumdar, A. Enhanced Thermopower in PbSe Nanocrystal Quantum Dot Superlattices. *Nano Lett.* **2008**, *8* (8), 2283−2288.
(25) Cai, Z.; Lo, W.-Y.; Zheng, T.; Li, L.; Zhang, N.; Hu, Y.; Yu, L. Exceptional Single-Molecule Transport Properties of Ladder-Type Heteroacene Molecular Wires. *J. Am. Chem. Soc.* **2016**, *138* (33), 10630−10635.
(26) Versnel, W. Analysis of Symmetrical Van Der Pauw Structures with Finite Contacts. *Solid-State Electron.* **1978**, *21* (10), 1261−1268.
(27) Lu, N.; Li, L.; Liu, M. Polaron Effect and Energetic Disorder Dependence of Seebeck Coefficient in Organic Transistors. *Org. Electron.* **2015**, *16*, 113−117.
(28) Remacle, F.; Collier, C. P.; Markovich, G.; Heath, J. R.; Banin, U.; Levine, R. D. Networks of Quantum Nanodots: The Role of Disorder in Modifying Electronic and Optical Properties. *J. Phys. Chem. B* **1998**, *102*, 7727−7734.
(29) Islam, M. F.; Nakanishi, H. Localization-Delocalization Transition in a Two-Dimensional Quantum Percolation Model. *Phys. Rev. E* **2008**, *77* (6), No. 061109.
(30) Emin, D. The Sign of the Hall Effect in Hopping Conduction. *Philos. Mag.* **1977**, *35* (5), 1189−1198.
(31) Frisch, M. J.; Trucks, G. W.; Schlegel, H. B.; Scuseria, G. E.; Robb, M. A.; Cheeseman, J. R.; Scalmani, G.; Barone, V.; Petersson, G. A.; Nakatsuji, H.; Li, X.; Caricato, M.; Marenich, A. V.; Bloino, J.; Janesko, B. G.; Gomperts, R.; Mennucci, B.; Hratch, D. J. *Gaussian 16*; Gaussian, Inc.: Wallingofrd, CT, 2016.
(32) Qi, J.; Edirisinghe, N.; Rabbani, M. G.; Anantram, M. P. Unified Model for Conductance through DNA with the Landauer-Büttiker Formalism. *Phys. Rev. B: Condens. Matter Mater. Phys.* **2013**, *87* (8), 085404.
(33) Kahn, A. Fermi Level, Work Function and Vacuum Level. *Mater. Horiz.* **2016**, *3* (1), 7−10.
(34) Scanlon, M. D.; Peljo, P.; Méndez, M. A.; Smirnov, E.; Girault, H. H. Charging and Discharging at the Nanoscale: Fermi Level Equilibration of Metallic Nanoparticles. *Chemical Science.* **2015**, *6*, 2705−2720.
(35) Snyder, G. J.; Ursell, T. S. Thermoelectric Efficiency and Compatibility. *Phys. Rev. Lett.* **2003**, *91* (14), 148301.
(36) McCold, C. E.; Fu, Q.; Howe, J. Y.; Hihath, J. Conductance Based Characterization of Structure and Hopping Site Density in 2D Molecule-Nanoparticle Arrays. *Nanoscale* **2015**, *7* (36), 14937−14945.
(37) McCold, C. E.; Fu, Q.; Hihath, S.; Han, J.; Halfon, Y.; Faller, R.; van Benthem, K.; Zang, L.; Hihath, J. Ligand Exchange Based Molecular Doping in 2D Hybrid Molecule-Nanoparticle Arrays: Length Determines Exchange Efficiency and Conductance Change. *Mol. Syst. Des. Eng.* **2017**, *2* (4), 440−448.
(38) Jonson, M.; Mahan, G. D. Mott's Formula for the Thermopower and the Wiedemann-Franz Law. *Phys. Rev. B: Condens. Matter Mater. Phys.* **1980**, *21* (10), 4223−4229.
(39) Graf, M. J.; Yip, S.-K.; Sauls, J. a.; Rainer, D. Electronic Thermal Conductivity and the Wiedemann-Franz Law for Unconventional Superconductors. *Phys. Rev. B: Condens. Matter Mater. Phys.* **1996**, *53* (22), 15147−15161.
(40) Cai, Z.; Zhang, N.; Awais, M.; Filatov, A.; Yu, L. Syntheses of Alternating Donor-Acceptor Ladder Type Molecules and Investigating Their Multiple Charge Transfer Pathways Modulated by Bandgap with STM-Break Junction. *Angew. Chem., Int. Ed.* **2018**, *57*, 6442.

DOI: 10.1021/acs.jpcc.9b08185
J. Phys. Chem. C 2020, 124, 17−24